


RESEARCH ARTICLE

Open Access



Daily and seasonal variations in the linear growth rate of the Rayleigh-Taylor instability in the ionosphere obtained with GAIA

Hiroyuki Shinagawa^{1*} , Hidekatsu Jin¹, Yasunobu Miyoshi², Hitoshi Fujiwara³, Tatsuhiro Yokoyama¹ and Yuichi Otsuka⁴

Abstract

The linear growth rates of the Rayleigh-Taylor (R-T) instability in the ionosphere from 2011 to 2013 were obtained with a whole atmosphere-ionosphere coupled model GAIA (ground-to-topside model of atmosphere and ionosphere for aeronomy). The effects of thermospheric dynamics driven by atmospheric waves propagating from below on the R-T growth rate are included in the model by incorporating meteorological reanalysis data in the region below 30 km altitude. The daily maximum R-T growth rates for these periods are compared with the observed occurrence days of the equatorial plasma bubble (EPB) determined by the Equatorial Atmosphere Radar (EAR) and Global Positioning System (GPS) in West Sumatra, Indonesia. We found that a high R-T growth rate tends to correspond to the actual EPB occurrence, suggesting the possibility of predicting EPB occurrences with numerical models.

Keywords: Equatorial plasma bubble, Occurrence rate, Daily variation, Atmosphere-ionosphere coupled model, Rayleigh-Taylor instability, Linear growth rate

Introduction

In recent years, the prediction of EPBs has been one of the most important issues in space weather forecasting because EPBs could adversely affect communication and navigation systems (e.g., Steenburgh et al. 2008; Sreeja 2016). Previous observational and theoretical studies have indicated that EPBs can be generated through the Rayleigh-Taylor (R-T) instability in the ionosphere (e.g., Scannapieco and Ossakow 1976; Woodman and LaHoz 1976; Ott 1978; Ossakow et al. 1979; Zalesak et al. 1982; Huba and Joyce 2007; Aveiro and Hysell 2010; Yokoyama et al. 2014, 2015). The flux tube integrated formulation of the equatorial ionosphere was given in several studies (e.g., Haerendel et al. 1992; Sultan 1996; Basu 2002). Among those studies, the formula of Sultan (1996) has been generally used to estimate the R-T growth rate. Recently, the R-T growth rate has been derived by Carter et al. (2014a, b) from the output data of the Thermosphere Ionosphere Electrodynamics General

Circulation Model (TIEGCM) (Richmond et al. 1992). They demonstrated that the R-T growth rate of EPBs is significantly controlled by geomagnetic activity. Carter et al. (2014a) also showed that the day-to-day quiet-time EPB occurrence observed in the Southeast Asian region agreed well with the result of TIEGCM for the 2000 March equinox period. Carter et al. (2014a, b) demonstrated that the geomagnetic activity (Kp index) is primarily responsible for the daily variability, and that even small changes in Kp have a significant effect on the occurrence of EPBs during the scintillation season.

Wu (2015) also used TIEGCM to show that the seasonal and longitudinal variations of the growth rate from the TIEGCM are consistent with the observed spread F variations, and that the growth rate is strongly dependent on the angle between the sunset terminator and the geomagnetic field line near the magnetic equator. Recently, Wu (2017) has investigated the solar effect on the R-T growth rate, and found that the correlation between $F_{10.7}$ and the R-T growth rate is unclear in a short time scale of less than 10 days.

Previous modeling studies, however, have not self-consistently incorporated actual day-to-day meteorological

* Correspondence: sinagawa@nict.go.jp

¹National Institute of Information and Communications Technology, Koganei, Tokyo 184-8795, Japan

Full list of author information is available at the end of the article

variations in the lower atmosphere, which drive various atmospheric waves propagating up to the thermosphere. Since the GAIA model is a “seamlessly coupled” whole atmosphere-ionosphere model with meteorological reanalysis data incorporated in the lower atmosphere, it is possible to obtain the daily variations of the R-T growth rate of EPBs related to the lower atmospheric variations.

In this paper, we use the GAIA model to examine the variations in the R-T growth rate and compare the values with the occurrence data derived from the Equatorial Atmosphere Radar (EAR) located at 0.20°S in geographic latitude (10.6°S in geomagnetic latitude), 100.32°E in geographic longitude, and from GPS observations at the same site. We focus on the day-to-day and seasonal variations in the R-T growth rate, which are key factors for the prediction of the EPB occurrence. The purpose of this study is to investigate how upper atmospheric variations in GAIA are related to EPB occurrence by comparing the model-derived R-T growth rate and the actual occurrence of EPBs at a given site.

Methods/Experimental

GAIA model

In the present analysis, we used the whole atmosphere-ionosphere coupled model GAIA to calculate the R-T growth rate in the ionosphere. GAIA consists of three models: an ionosphere model, a neutral atmosphere model, and an ionospheric electrodynamic model. In the neutral atmosphere model, hydrodynamic equations are solved by the spectral method. The spatial resolution is equivalent to a grid size of 2.8° longitude by 2.8° latitude in the horizontal direction, and 0.2 scale height in the vertical direction. The neutral atmosphere model covers the entire atmospheric region from the surface up to the top of the thermosphere, which is about 500 km altitude. The effects of all basic physical processes in the atmosphere such as surface topography, radiative processes, eddy and molecular diffusion processes, and moist convection are included in the model (Fujiwara and Miyoshi 2009, 2010; Miyoshi and Fujiwara 2003, 2006, 2008; Miyoshi et al. 2012, 2014). At altitudes below 30 km, the meteorological reanalysis data JRA-25 (Japanese 25-year Reanalysis) are incorporated into the simulation model by a nudging method (Jin et al. 2012). This procedure enables us to incorporate actual meteorological processes in the lower atmosphere as well as various atmospheric waves generated at lower altitudes. Another input to the model is the $F_{10.7}$ index, which is taken from NOAA/NCEI.

In the ionospheric model, plasma fluid equations for several major ion species and electrons are solved using the finite difference scheme. The spatial grid intervals are of 2.5° longitude by 1° latitude horizontally. The vertical

grid interval is 10 km below 600 km, and at altitudes higher than 600 km, the grid interval increases gradually up to 100 km at the upper boundary of 3000 km. In the ionospheric electrodynamic model, the global electrostatic potential driven by neutral winds is calculated assuming that geomagnetic field lines are equipotential and the current is closed within the ionosphere region (Jin et al. 2008, 2011, 2012). In the present analysis, the GAIA model incorporates a quiet magnetospheric condition with a constant cross polar cap potential, which is 30 kV. Therefore, the effect of a varying geomagnetic activity level is not included in the present study.

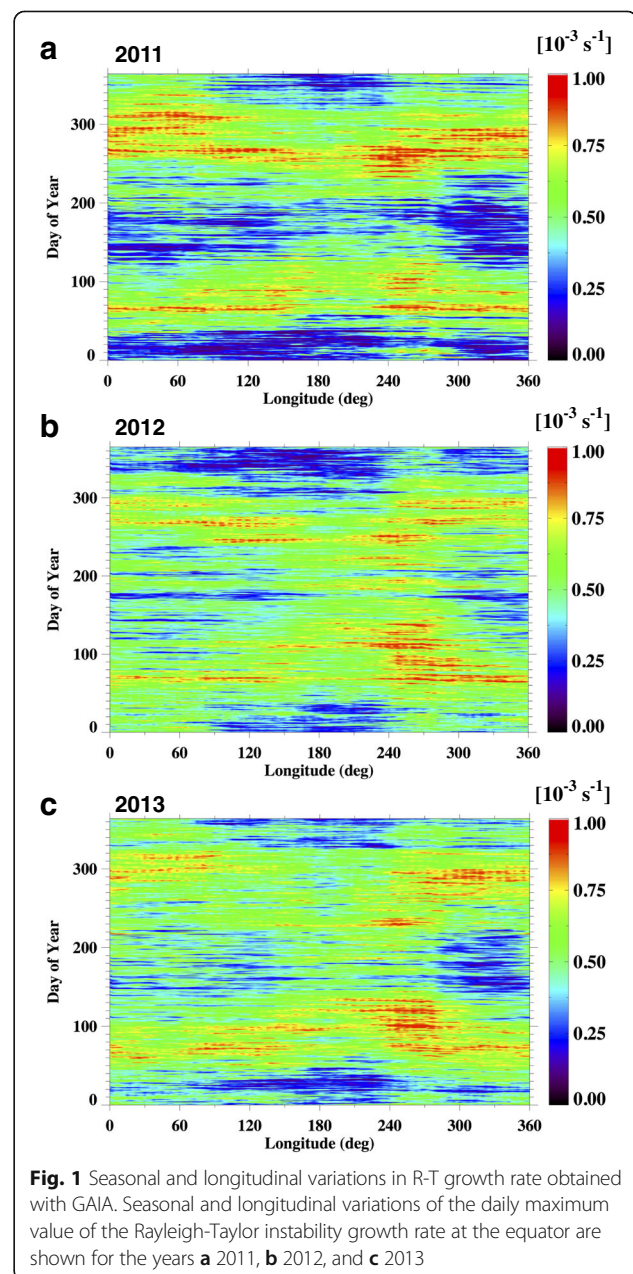


Fig. 1 Seasonal and longitudinal variations in R-T growth rate obtained with GAIA. Seasonal and longitudinal variations of the daily maximum value of the Rayleigh-Taylor instability growth rate at the equator are shown for the years **a** 2011, **b** 2012, and **c** 2013

Calculation of R-T growth rate using GAIA

We adopted the formula of Sultan (1996), in which the flux tube integrated linear R-T growth rate γ is expressed as

$$\gamma = \frac{\Sigma_p^F}{\Sigma_p^E + \Sigma_p^F} \left(V_p - U_L^p - \frac{g_e}{v_{\text{eff}}^F} \right) K^F - R_T, \quad (1)$$

where Σ_p^F and Σ_p^E are the flux tube integrated Pedersen conductivities in the F region and the E region, respectively, V_p is the vertical component of plasma drift due to the zonal component of the electric field \mathbf{E} at the magnetic equator, U_L^p is the neutral wind perpendicular to the magnetic field in the magnetic meridian plane weighted by the Pedersen conductivity, g_e is the downward gravity acceleration, v_{eff}^F is the flux tube integrated effective ion-neutral collision frequency weighted by the electron number density, K^F is the altitude gradient of flux tube integrated electron content in the F region,

and R_T is the flux tube integrated recombination rate weighted by the electron number density.

Using Eq. (1), the R-T growth rate was calculated for the magnetic flux tubes above the EAR site, at every 10 km in altitude every 30 min for each day, and the highest R-T growth rate among all local times and altitudes at the site was adopted for the day, which usually occurs in the evening in the F region. As mentioned in the previous section, the effects of variations in geomagnetic activity are not included in the present analysis. Therefore, only the effects of atmospheric variations, $F_{10.7}$ variations, seasonal variations, and atmospheric waves propagating from the lower atmosphere are included.

Observation data of EPBs

To compare the calculated R-T growth rate with the actual EPB occurrence, we used two types of observation data in our analysis: one is the field-aligned irregularity (FAI) data derived from EAR (Fukao et al. 2004; Otsuka

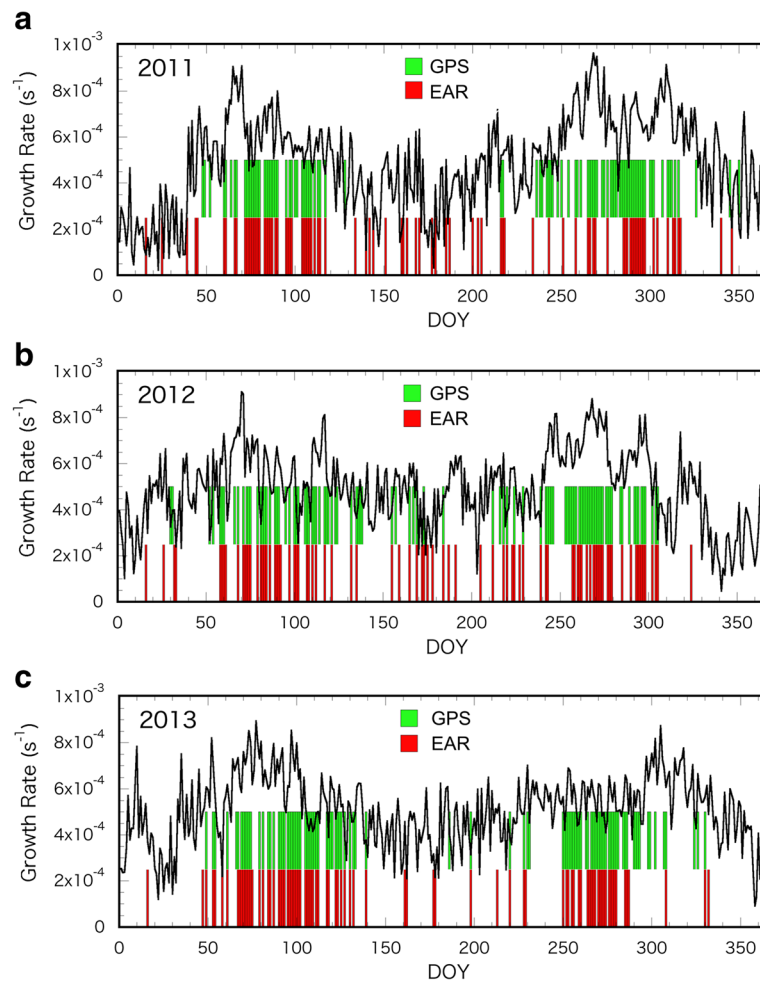


Fig. 2 Daily variations in R-T growth rate obtained with GAIA. The daily maximum values of the R-T growth rate (black line) are obtained with GAIA at 100°E for the years of **a** 2011, **b** 2012, and **c** 2013. Vertical bars indicate the days when EPBs are detected by EAR (red bar) and by GPS (green bar)

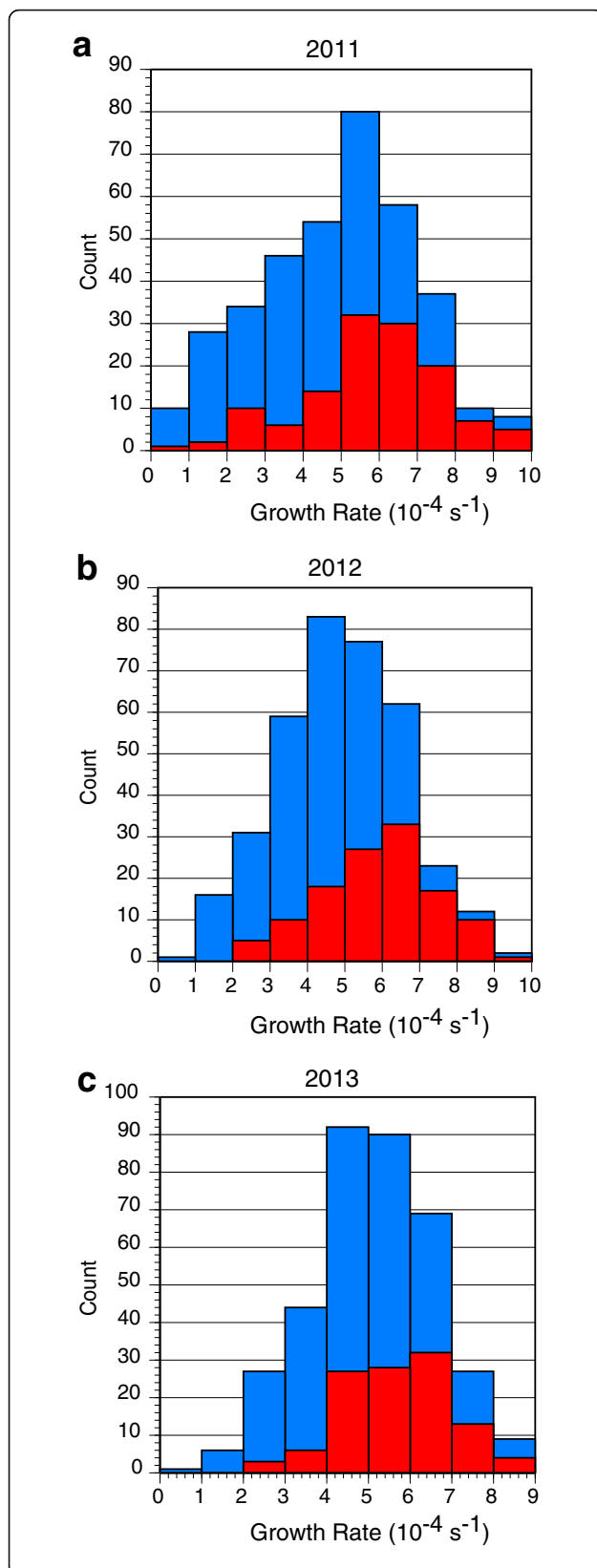


Fig. 3 Histograms of the number of EPB occurrence and non-occurrence days for the R-T growth rate. The histograms indicate the relationship between the number of days of EPB occurrence and non-occurrence and the R-T growth rate in **a** 2011, **b** 2012, and **c** 2013. The values of the R-T growth rate are split into 10 bins with a width of 10^{-4} s^{-1} . Red bars are the numbers of days when EPBs are observed, and blue bars are the numbers of days when EPBs are not observed

et al. 2004), and the other is the S_4 index data derived from GPS data (Otsuka et al. 2006; Ogawa et al. 2009). Since both FAI data and S_4 index data are considered to be good indicators of EPBs, an occurrence data set was generated using the two types of data.

The EAR, located at Kototabang (0.20°S; 100.3°E), Indonesia, is a large monostatic radar operating at 47.0 MHz with a peak output power of 100 kW. By steering the radar beam in 16 directions perpendicular to the geomagnetic fields, 3-m scale FAIs are observed in a fan-shaped range azimuth sector (fan sector) map that covers 600 km in the zonal direction at an altitude of 450 km (Fukao et al. 2004) approximately every 2 min. Since July 2010, FAI measurements have been carried out routinely every night. Otsuka et al. (2004) have shown that FAI with a signal-to-noise ratio larger than 0 dB coincides well with plasma depletion observed in the 630-nm airglow image taken by an all-sky airglow imager installed at the EAR site. Typically, FAI regions have a zonal width of 100–200 km and propagate eastward at a velocity of 40–140 m/s (Fukao et al. 2006). Therefore, the FAIs are detected on a fixed beam for 10–80 min. In this study, FAI occurrence is defined as an event in which FAIs with signal-to-noise ratios larger than 0 dB continue for more than 10 min.

At the EAR site, three single-frequency GPS receivers have been operated since January 2003 (Otsuka et al. 2006; Ogawa et al. 2009) to measure amplitude scintillation. GPS scintillation at the equatorial region could be caused by plasma density irregularities within EPBs. The signal intensity of the GPS L1 frequency (1.57542 GHz) is measured at a rate of 20 Hz. The scintillation index S_4 , defined as the standard deviation of signal intensities divided by their mean, is obtained every minute. To avoid the multipath effects of GPS signals, the data with elevation angles less than 30° were excluded (Otsuka et al. 2006). We average S_4 over 10 min and selected the highest S_4 among all the 10-min S_4 values obtained for different satellites simultaneously. To investigate the day-to-day variation of S_4 , the 10-min S_4 values are averaged over a period from 1900 to 2400 LT. In this study, we define the day of EPB occurrence as the day when the daily S_4 is larger than 0.3.

We compare the model-derived R-T growth rate with the observed EPB occurrence data for the years 2011–2013. This is because complete data of the EPB

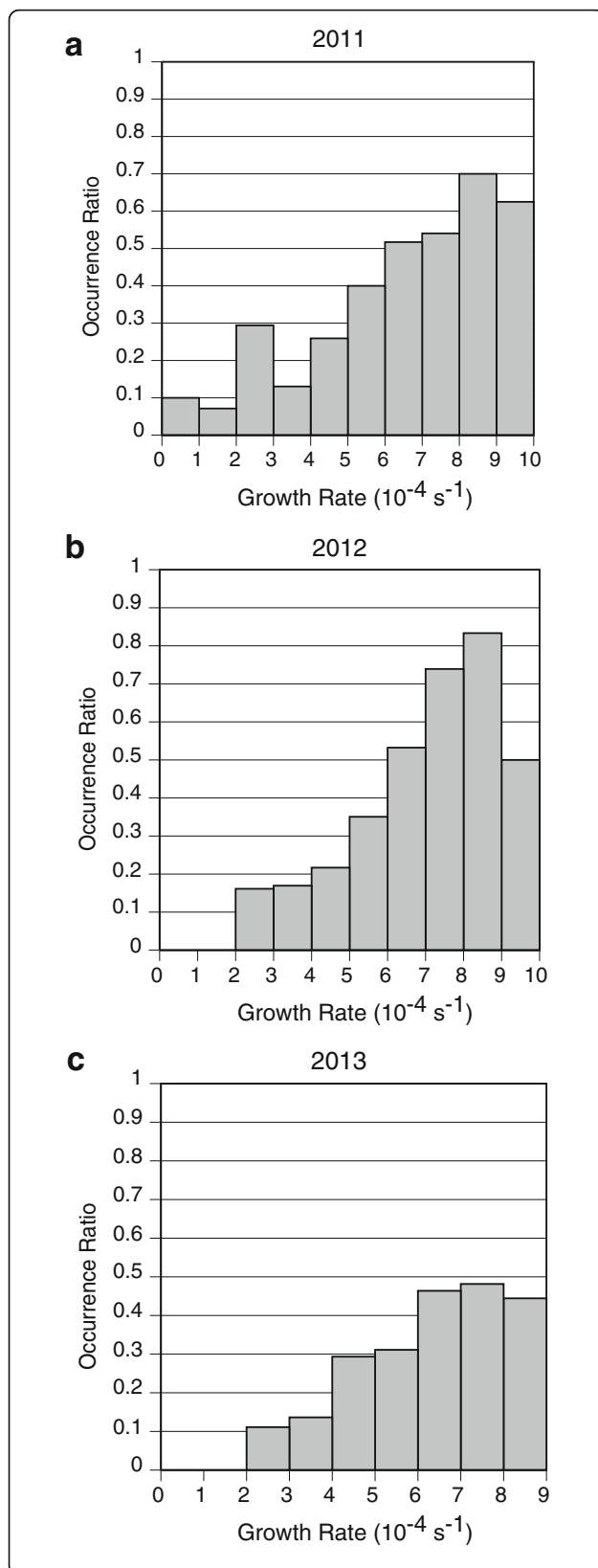


Fig. 4 Histograms of the number of EPS occurrence/non-occurrence days for the R-T growth rate. The histograms indicate the relationship between the rate of days of EPB occurrence and the R-T growth rate in **a** 2011, **b** 2012, and **c** 2013

occurrence is available for both FAI and S_4 index data for these 3 years. As will be explained later, the EPB occurrence days identified by the two observations do not agree with each other on some days especially in the June solstice periods. FAIs occurring in the June solstice period appear more frequently at post-midnight and is not accompanied by GPS scintillation (e.g., Otsuka et al. 2009, 2012; Nishioka et al. 2012). This is one of the reasons behind the disagreement between the two observations. The disagreement in equinox season appears to come from the differences in the accuracy and direction of the measurement. In this study, “the occurrence day” means the day when EPB is identified either by EAR or GPS. The occurrence days are compared with the model-derived R-T growth rates.

Results

Longitudinal-seasonal variations in R-T growth rate

Figure 1 shows contour plots of daily maximum R-T growth rates for different longitudes and day of year for the years 2011–2013 in the unit of 10^{-3} s^{-1} . Seasonal and longitudinal variations in the R-T growth rate are clearly seen for all these 3 years. The R-T growth rate peaks in the two equinox periods for all longitudes except in the central Pacific region, where the growth rate peaks are unclear. Although the overall pattern is roughly consistent with the EPB occurrence rates derived from satellite observations (Watanabe and Oya 1986; Burke et al. 2004a, b; Gentile et al. 2006; Nishioka et al. 2008; Kil et al. 2009; Huang et al. 2014, Huang and Hairston 2015), there are some discrepancies between the R-T growth rate and the observed occurrence rate. One notable difference is that in the observed occurrence rates, there is a clear maximum in the Atlantic region (Burke et al. 2004a, b), while the maximum is not very clear in the R-T growth rate in GAIA. This is probably because GAIA employs a tilted dipole model, which significantly differs from the real magnetic field configuration in that region. In the central Pacific region, the peak R-T growth rate is less significant than in other regions, which is consistent with the observations (Burke et al. 2004a, b; Gentile et al. 2006; Nishioka et al. 2008).

Day-to-day variations in R-T growth rate and EPB occurrence

In addition to seasonal and longitudinal variations in the maximum R-T growth rate, Fig. 1 shows significant day-to-day variations throughout the year at all longitudes.

Since in the present analysis we did not include variations in the polar energy inputs from the magnetosphere, day-to-day variations in the R-T growth rate are caused by day-to-day variations in neutral winds and densities and in ionospheric conductivities, which are associated with solar EUV/X-ray radiation ($F_{10.7}$ index) and atmospheric waves propagating from the lower atmosphere.

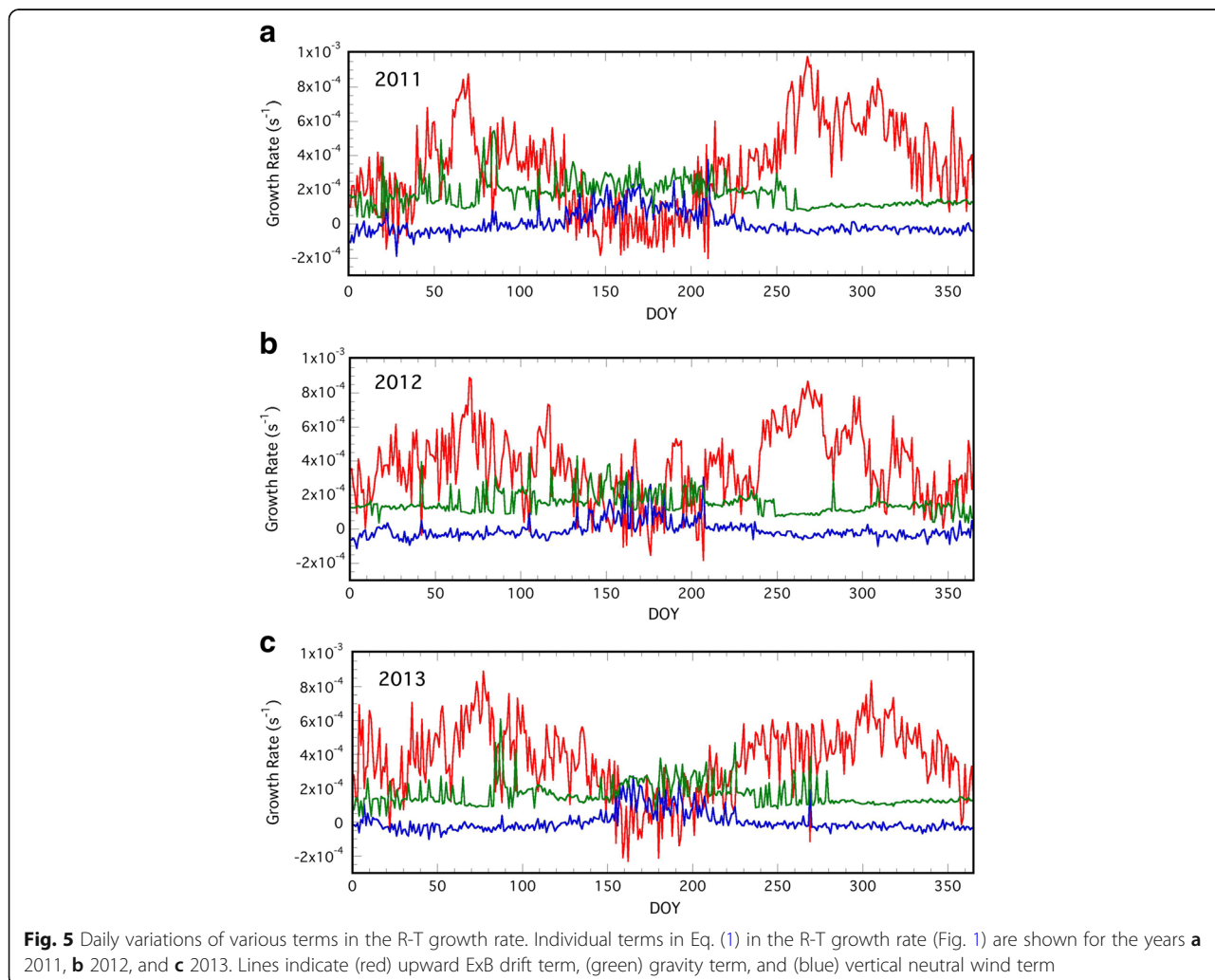
In Fig. 2, day-to-day variations in the R-T growth rate at 100°E longitude are compared with the EPB occurrence observations at the EAR site in 2011–2013. The vertical axis is the R-T growth rate in the unit of 10^{-3} s^{-1} , and the horizontal axis is the day of year (DOY). The red lines indicate the daily maximum R-T growth rates calculated with GAIA. The vertical bars indicate the days when a plasma bubble is detected by EAR (green bar) and by GPS (red bar).

In all the 3 years, seasonal variations are clearly seen in both the daily R-T growth rate and EPB occurrence, which are maximum in the two equinoxes. For daily variations, there is a relatively good correlation between the observed occurrence days and the days with a large

R-T growth rate, although there are some periods of disagreement.

In the year 2011 (Fig. 2a), few EPBs were detected until DOY 40. From DOY 1 to DOY 40, the R-T growth rate is relatively low. Between DOY 40 and DOY 120, EPBs appear very often and the R-T growth rate is also high. After DOY 120, the EPB occurrence suddenly becomes sporadic and detected only by EAR until DOY 230. The calculated R-T growth rate is generally low except for an occasional enhancement, which does not always agree with the observed occurrence days. After DOY 230, EPBs are frequently seen again until DOY 318, while the R-T growth rate is also high during this period. After DOY 318, EPB activity decreases rapidly, and the R-T growth rate also decreases with increases on some days, for which the agreement with the EPB occurrence is not good.

In the year 2012 (Fig. 2b), EPBs are observed occasionally on DOYs 15–32 unlike in the same period in 2011. The R-T growth rate increases from the beginning of the year and is relatively high during the same period.



Between DOY 50 and DOY 140, EPBs occur frequently, and their occurrence days seem to correspond to the days with high R-T growth rates. During the months around the June solstice (DOYs 150–240), EPBs are seen relatively often. The R-T growth rate is also fairly high compared with that in the same period in 2011, but the agreement between the R-T growth rate and the EPB occurrence rate is not very good. After DOY 240, the EPB occurrence rate becomes high again, and the occurrence days tend to agree with the days with high R-T growth rates. After DOY 305, EPB is observed only once by EAR on DOY 324, on which the R-T growth rate is relatively high. Although the R-T growth rate is high on DOYs 317, 320, and 329, no EPB has been observed on those days.

In the year 2013 (Fig. 2c), EPB is detected only once before DOY 47, while the R-T growth rate becomes high between DOY 5 and DOY 15 and between DOY 33 and DOY 47, which is not consistent with the observations.

As in 2011 and 2012, the observed occurrence rate of EPB is high in the equinox months. The R-T growth rate is also high during the periods, but the individual occurrence days are not in good agreement for this year. Around the two solstices, the agreement is also not as good as those in 2011 and 2012.

Overall, the R-T growth rate derived from GAIA simulation data exhibits clear seasonal and day-to-day variations. A high R-T growth rate tends to correspond to the observed occurrence days determined by EAR and GPS measurements during the two equinox periods, while in the two solstice periods, the agreement is worse, especially in 2013.

Discussion

Relationship between EPB occurrence and R-T growth rate

In the previous section, we found that there appears to be a fairly good relationship between the EPB occurrence and

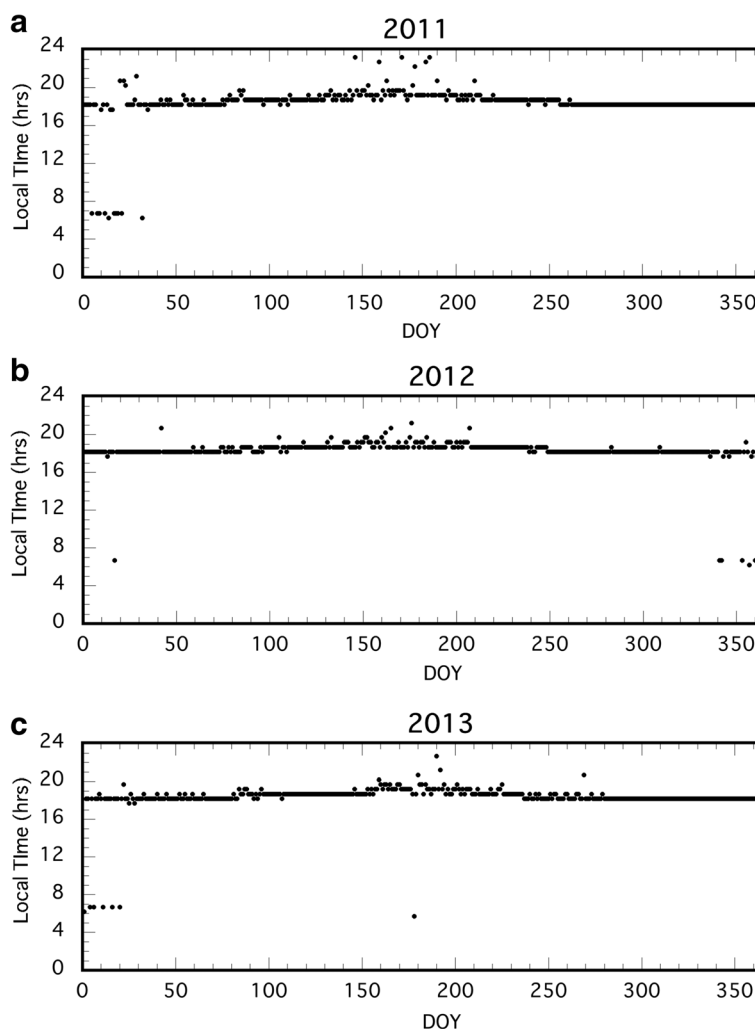


Fig. 6 Local time of the maximum R-T growth rate occurrence. Black circles indicate the local times when the maximum R-T growth rate occurred in **a** 2011, **b** 2012, and **c** 2013

the R-T growth rate. To show the relationship more quantitatively, histograms of the number of days of EPB occurrence and non-occurrence sorted by the R-T growth rate are plotted in Fig. 3. The R-T growth rates are split into bins with a width of 10^{-4} s^{-1} . Red bars indicate the number of days of EPB occurrence, and blue bars indicate the number of days of non-occurrence. Figure 4 shows histograms revealing the relationship between the rate of days of EPB occurrence and the R-T growth rate. The result clearly shows that EPB tends to occur more frequently as the R-T growth rate increases, although the correlation is weaker in 2013 than in 2011 and 2012.

Processes controlling variations in R-T growth rate

Figure 2 indicates that the R-T growth rate varies significantly in various time scales. To study which processes control the variations in the total R-T growth rate, we examined each term in Eq. (1). Figure 5 shows the variations in the terms of the R-T growth rate at 100°E for the years (a) 2011, (b) 2012, and (c) 2013. The red line is the upward $\mathbf{E} \times \mathbf{B}$ drift term $[\Sigma_p^F / (\Sigma_p^E + \Sigma_p^F)] V_p K^F$; the blue line is the vertical neutral wind term $-[\Sigma_p^F / (\Sigma_p^E + \Sigma_p^F)] U_L^P K^F$; the

green line is the gravity term $-[\Sigma_p^F / (\Sigma_p^E + \Sigma_p^F)] (g_e / v_{eff}^F) K^F$. The chemical recombination term R_T is much smaller than other terms where the maximum R-T growth rate occurs, and therefore is not plotted in Fig. 5.

Figure 5 indicates that the $\mathbf{E} \times \mathbf{B}$ term (red line) primarily contributes to the R-T growth rate most of the time, as was pointed in previous studies (Carter et al. 2014a, b; Wu 2015, 2017). Since our present analysis includes low and fixed polar energy inputs, the electric field variations arise from neutral wind variations driven by atmospheric waves propagating from the lower atmosphere. Variations in the electric field are also caused by variations in electric conductivities and angles between magnetic field lines and the terminator line. The gravity term occasionally becomes large and makes a significant contribution.

The term of the vertical-meridional component of the neutral wind perpendicular to the magnetic field U_L^P (blue line) tends to become larger after the March equinox and during June solstice periods. Variations in thermospheric winds are closely associated with atmospheric waves propagating from the troposphere (Miyoshi et al. 2017), which have significant seasonal dependence. In general, the larger meridional component of the

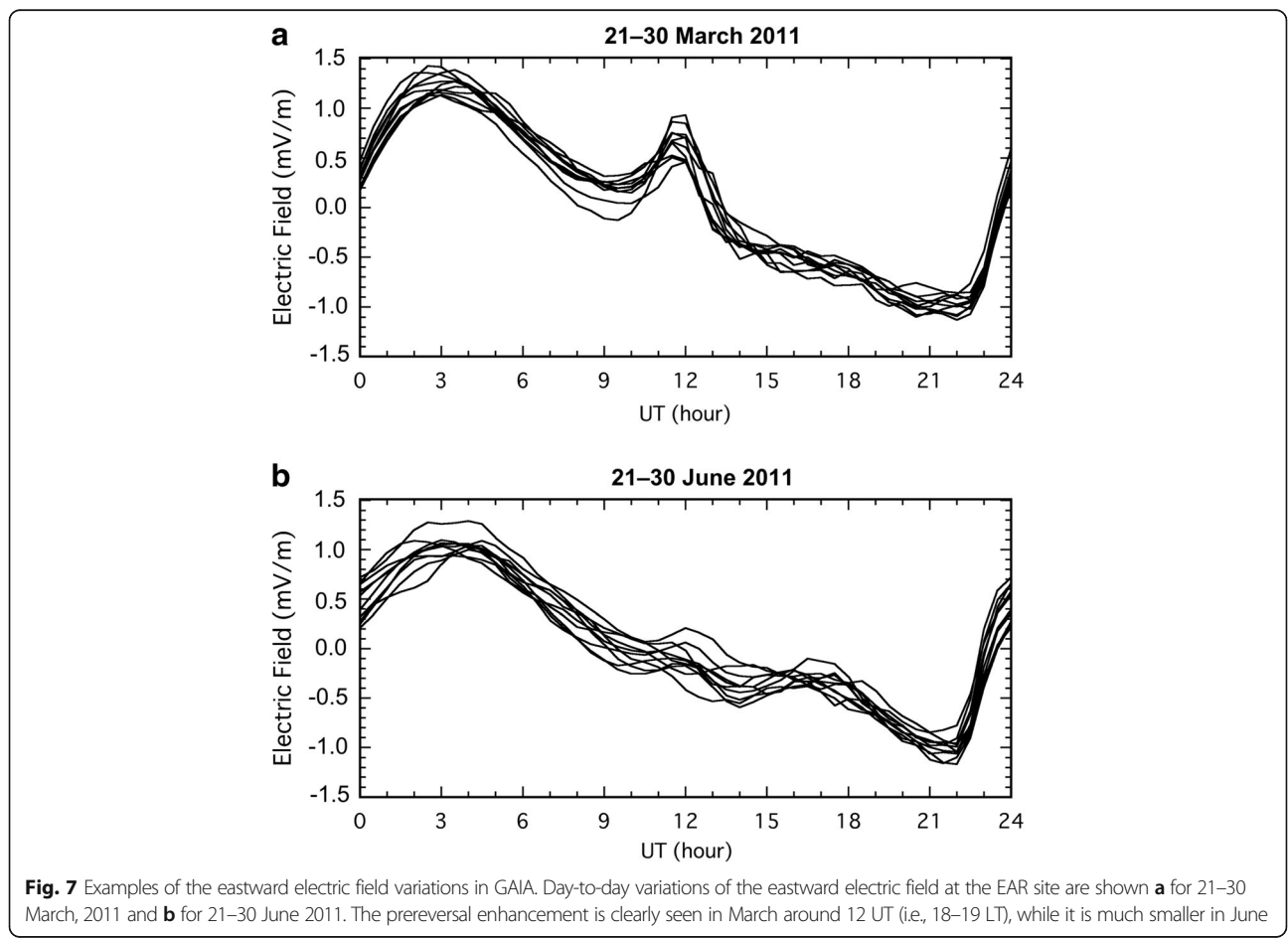


Fig. 7 Examples of the eastward electric field variations in GAIA. Day-to-day variations of the eastward electric field at the EAR site are shown **a** for 21–30 March, 2011 and **b** for 21–30 June 2011. The prereversal enhancement is clearly seen in March around 12 UT (i.e., 18–19 LT), while it is much smaller in June

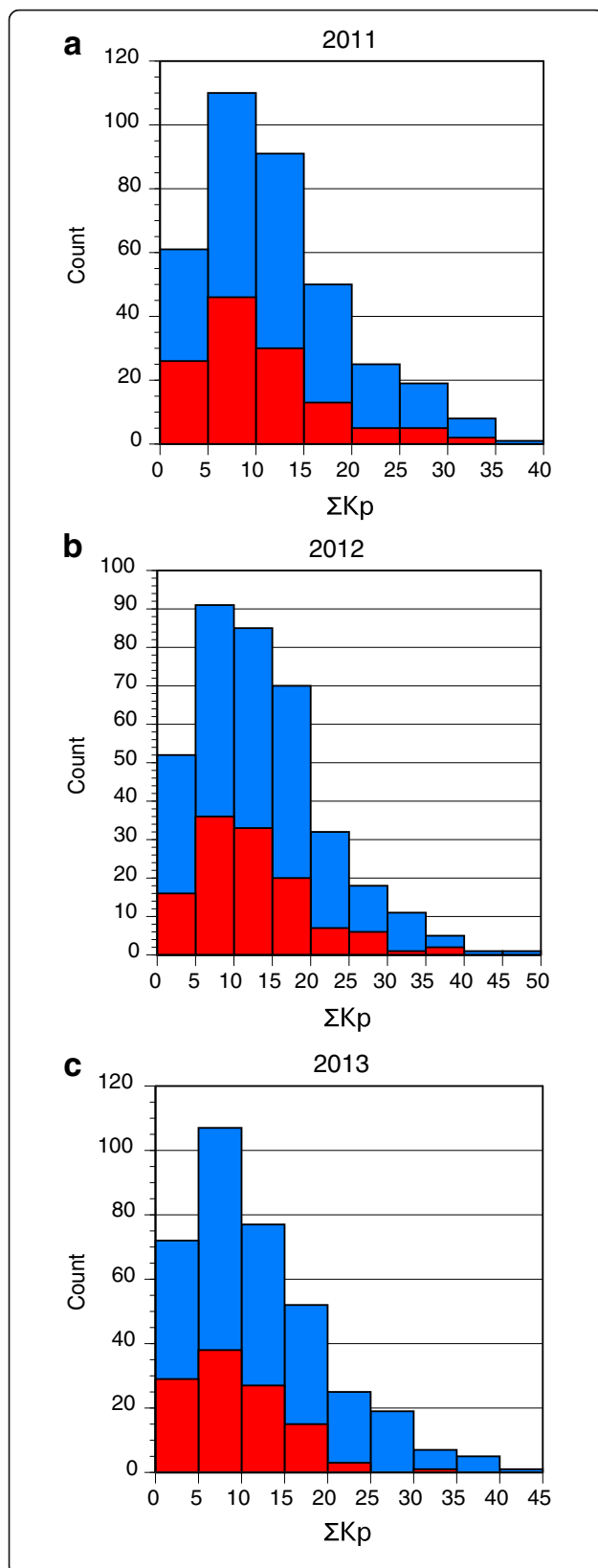


Fig. 8 Histograms of the number of EPB occurrence/non-occurrence days for ΣKp . The histograms indicate the relationship between ΣKp (daily total of the Kp) and the number of days of EPB occurrence (red bars) and non-occurrence (blue bars) in **a** 2011, **b** 2012, and **c** 2013

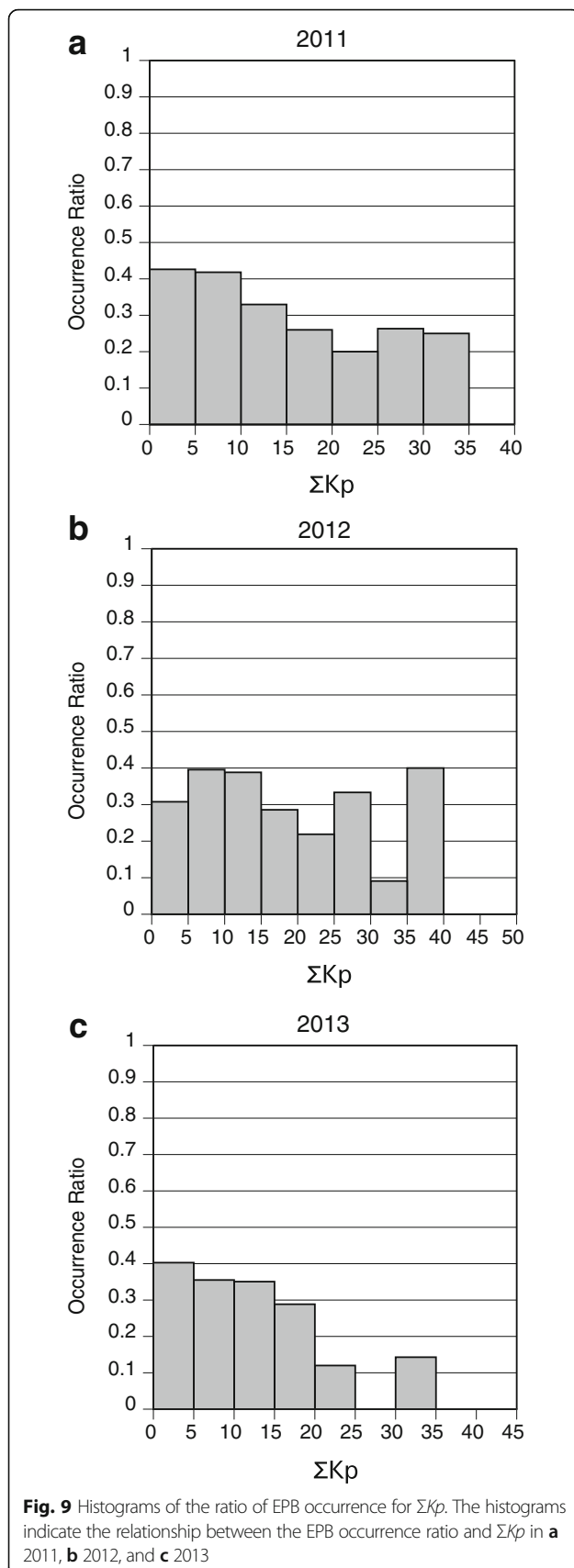
thermospheric wind contributes to the larger value of the term. However, the variation in the u_L^p term is extremely complicated because it is a flux tube integrated quantity of the vertical-meridional component of neutral winds perpendicular to the magnetic field. Furthermore, thermospheric winds usually vary significantly near the terminator. Since the behavior of the neutral wind term becomes occasionally important around the June solstice, reproducing thermospheric winds accurately is the key to the analysis using the R-T growth rate. The results show that all terms except the chemical recombination term are highly variable and have significant contributions to the R-T growth rate especially in the June solstice.

Figure 6 indicates the local time when the maximum R-T growth rate occurred at the EAR site. The maximum R-T growth rate occurs around 18–19 LT most of the days. In the June solstice, the maximum R-T growth rate tends to appear in later hours than in other seasons, as pointed out in previous studies (e.g., Otsuka et al. 2009; Ajith et al. 2016). This is because the prereversal enhancement (PRE) is weaker during the period. Figure 7 shows the eastward electric field variations at the EAR site during 21–30 March 2011 and 21–30 June 2011. The PRE is clearly seen in March around 12 UT (i.e., 18–19 LT at the EAR site), while it is much smaller in June.

Effects of geomagnetic activity on R-T growth rate

Carter et al. (2014a, b) showed that geomagnetic activity influences EPBs, and that EPB development tends to be suppressed as a result of geomagnetic activity. Since the present GAIA model does not include the effect of varying polar energy inputs, we examined the relationship between geomagnetic activity and EPB occurrence by comparing ΣKp and the plasma bubble occurrence at the EAR site for the years 2011–2013. Figure 8 shows histograms of the numbers of EPB occurrence days (red bars) and non-occurrence days (blue bars) sorted by ΣKp (daily total of Kp) in the years 2011–2013. Figure 9 shows histograms of ΣKp for the ratios of EPB occurrence days in the years 2011–2013. Values of ΣKp are split into bins with a width of 5.

The result indicates that the EPB occurrence ratio tends to decrease as ΣKp increases, which is consistent with the result obtained by Carter et al. (2014b). However, the dependence of the occurrence ratio on ΣKp is not very clear for ΣKp larger than about 25, suggesting that strong geomagnetic activity occasionally induces EPB development (Basu et al. 2007; Tulasi Ram et al. 2008;



Huang 2011). Since the present version of GAIA does not include varying polar inputs, the effects of geomagnetic activity are not included in our present study.

Effect of solar EUV/X-ray radiation on the R-T growth rate

Figure 10 shows the day-to-day variations in the R-T growth rate and $F_{10.7}$ for the years 2011–2013. In 2011 (Fig. 4a), the R-T growth rate and $F_{10.7}$ show similar seasonal variations in which they are maximum in the two equinoxes. This agreement appears to be coincidental because solar activity usually does not have seasonal variations as seen in 2012 and 2013. The agreement between the R-T growth rate and $F_{10.7}$ is unclear on a short time scale (< 10 days). This is similar to the result given by Wu (2017) who used TIEGCM to obtain the R-T growth rate. Wu (2017) mentioned that the weak correlation between the R-T growth rate and $F_{10.7}$ is due to the fact that the field-line integrated electron content gradient cancels out the positive correlation between the vertical ion drift and the $F_{10.7}$ index. On the other hand, previous statistical analyses indicated that there are significant correlations between plasma bubble occurrences and $F_{10.7}$ (Watanabe and Oya 1986; Huang et al. 2002; Nishioka et al. 2008), although the correlation depends on various parameters such as longitude, local time, and year. In our analysis, there appear to be some periods in which there are relatively good correlations between the R-T growth rate and $F_{10.7}$, especially in the latter half of 2012. In 2012, variations of the 27-day period are seen in GRT and $F_{10.7}$ between DOY 180 and DOY 310 (Fig. 10b). It seems that a very large $F_{10.7}$ tends to increase the R-T growth rate.

On disagreement between R-T growth rate and EPB occurrence

Although the R-T growth rate agrees with the EPB occurrence for some periods, significant discrepancies are present. There seem to be three factors that lead to the discrepancies: (1) measurement problems, (2) errors in GAIA model, and (3) applicability of the R-T growth rate for the EPB occurrence index.

In this study, we have used the FAI observed by the EAR and the GPS scintillation observed by a GPS receiver at the EAR site to detect the plasma bubble occurrence. As shown in Fig. 2, the FAI occurrence is not always consistent with the GPS scintillation occurrence. This discrepancy could be attributed mainly to the following two reasons. (1) Since EAR is located at the magnetic latitude of 10.4°S, plasma bubbles that do not reach the latitude of the EAR are not observed. FAIs are mostly observed with the EAR at altitudes higher than 250 km. The apex altitude of the field-of-view of

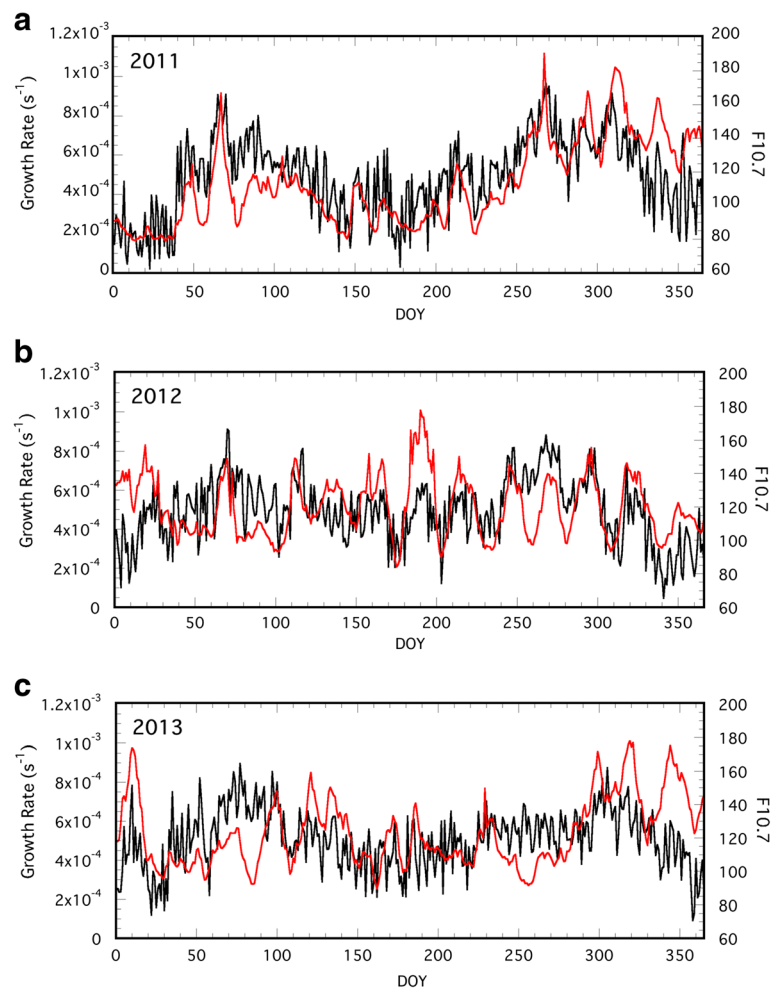


Fig. 10 Daily variations in R-T growth rate and the observed daily $F_{10.7}$. The R-T growth rate in GAIA at 100°E and the observed daily $F_{10.7}$ are shown for **a** 2011, **b** 2012, and **c** 2013. Black lines indicate the daily maximum values of the R-T growth rate and red lines indicate the daily values of $F_{10.7}$

the EAR at a 250-km altitude is 420 km (Dao et al. 2016). Consequently, no plasma bubbles that are confined at an apex altitude lower than 420 km are detected with the EAR. On the other hand, the GPS scintillation measurement covers an area within a zenith angle of less than 60° , i.e., an area within a radius of approximately 470 km, and thus the plasma bubbles that do not reach the field-of-view of the EAR can be observed with the GPS measurements. (2) The ionospheric pierce points of the ray path of GPS radio waves move either from SSW to NNE or from NNW to SSE at approximately 100 m/s. Plasma bubbles immediately after sunset move eastward at 100–150 m/s on average (e.g., Otsuka et al. 2006). Since the movements of both the ionospheric pierce points and plasma bubbles have an eastward component, it is possible that the pierce points cannot come across the plasma bubbles although multiple satellites are available simultaneously, implying that GPS measurements at a single site may miss the plasma bubble occurrence.

Consequently, in this study, we have used both FAIs and GPS scintillations and defined the day of plasma bubble occurrence as the day when either the FAIs or GPS scintillations are detected.

As mentioned earlier, the present analysis does not include the effect of magnetic disturbances, which are thought to control the occurrence of EPBs. Carter et al. (2014a, b) showed that geomagnetic activity is one of the key parameters for the occurrence of EPBs. Thus, it is necessary to include this effect to further improve the reproducibility of EPB occurrence. In addition, the present GAIA model employs a tilted dipole magnetic field model, which seems to give some errors in the R-T growth rate. There is likely to be some uncertainties in reproducing thermospheric neutral winds, which are parameters essential to ionospheric dynamo processes.

Although the linear growth rate of the Rayleigh-Taylor instability appears to be a good index of the plasma bubble occurrence, a high R-T growth rate does not

necessarily mean a fully developed EPB structure. Even if the R-T growth rate becomes high instantaneously, EPBs do not grow unless a high R-T growth rate continues for 1 or 2 h. It is also likely that an EPB is produced somewhere else and drifts into the observation site. As studied by Ajith et al. (2015), there are two types of EPBs: evolving-type EPBs and drifting-in EPBs, suggesting that EPBs can be observed even if the R-T growth rate is low.

Prediction of EPB occurrence

Our study as well as other previous studies (e.g., Carter et al. 2014a, b; Wu 2015, 2017) suggest that the R-T growth rate calculated with numerical models could be a good index for the prediction of EPBs. However, we have compared past EPB occurrence data and R-T growth rates calculated with GAIA and past meteorological reanalysis data. For the practical forecast of EPBs, it is necessary to predict ionosphere-thermosphere variations one or more days ahead. One possible way to make a prediction is to introduce meteorological forecast data instead of the meteorological reanalysis data in the lower atmosphere. The other way is to run GAIA by itself without the meteorological reanalysis data. Since GAIA can reproduce meteorological processes in the troposphere to some degree, it is expected that the model can be used to predict the atmosphere-ionosphere system without forecast data. Further investigation is necessary for the development of a forecast technique.

Conclusion

The daily maximum R-T growth rates were obtained from GAIA simulation data, and were compared with the EPB occurrence data obtained from two types of observations: FAIs of EAR and S4 index from the GPS receiver for the years 2011–2013. This is the first paper to quantify the effect of lower atmospheric forcing on the R-T growth rate in the ionosphere. The results show that a high R-T growth rate tends to correspond to the actual occurrence of EPB. Although the effect of varying magnetic activity is not included in the present analysis, the results of the present study indicate that lower atmospheric forcing is an important process in controlling the R-T growth rate, suggesting that the R-T growth rate is a useful index for the prediction of EPB occurrence.

Abbreviations

DOY: Day of year; EAR: Equatorial Atmosphere Radar; EPB: Equatorial plasma bubble; EUV: Extreme ultraviolet; FAI: Field-aligned irregularity; GAIA: Ground-to-topside model of Atmosphere and Ionosphere for Aeronomy; GPS: Global Positioning System; JRA-25: Japanese 25-year Reanalysis; NCEI: National Centers for Environmental Information; NOAA: National Oceanic and Atmospheric Administration; PRE: Prereversal enhancement; R-T: Rayleigh-Taylor; TIEGCM: Thermosphere Ionosphere Electrodynamics General Circulation Model

Acknowledgements

Simulations and data analyses in this work were performed using Hitachi SR16000/M1 and the NICT Science Cloud System, Japan. Numerical simulation in this study was also performed as a computational joint research program at the Institute for Space-Earth Environmental Research, Nagoya University, Japan. The meteorological reanalysis data was obtained from the cooperative research project of the JRA-25 long-term reanalysis by the Japan Meteorological Agency (JMA) and the Central Research Institute of Electric Power Industry (CRIEPI) (<http://www.jreap.org/indexe.html>). The F10.7 index data was obtained from NOAA/NCEI. K_p index data was obtained from World Data Center for Geomagnetism, Kyoto.

Funding

This work is supported by JSPS KAKENHI Grant Numbers JP15H03733 and JP15H05815.

Authors' contributions

HS proposed the topic and analyzed the data of GAIA simulation. HS, HJ, YM, and HF developed the GAIA model. HJ and YM carried out simulation and created the simulation database. YO analyzed the observation data and created EPB occurrence data. TY gave information on the physics of EPB. All authors read and approved the final manuscript.

Competing interests

The authors declare that they have no competing interests.

Publisher's Note

Springer Nature remains neutral with regard to jurisdictional claims in published maps and institutional affiliations.

Author details

¹National Institute of Information and Communications Technology, Koganei, Tokyo 184-8795, Japan. ²Department of Earth and Planetary Sciences, Kyushu University, Fukuoka 819-0395, Japan. ³Faculty of Science and Technology, Seikei University, Musashino, Tokyo 180-8633, Japan. ⁴Institute for Space-Earth Environmental Research, Nagoya University, Nagoya 464-0814, Japan.

Received: 30 August 2017 Accepted: 22 February 2018

Published online: 09 March 2018

References

- Ajith KK, Tulasi Ram S, Yamamoto M, Otsuka Y, Niranjan K (2016) On the fresh development of equatorial plasma bubbles around the midnight hours of June solstice. *J Geophys Res Space Physics* 121:9051–9062. <https://doi.org/10.1002/2016JA023024>
- Ajith KK, Tulasi Ram S, Yamamoto M, Yokoyama T, Gowtam VS, Otsuka Y, Sugawa T, Niranjan K (2015) Explicit characteristics of evolutionary-type plasma bubbles observed from equatorial atmosphere radar during the low to moderate solar activity years 2010–2012. *J Geophys Res Space Physics*:120. <https://doi.org/10.1002/2014JA020878>
- Aveiro HC, Hysell DL (2010) Three-dimensional numerical simulation of equatorial F region plasma irregularities with bottomside shear flow. *J Geophys Res* 115:A11321. <https://doi.org/10.1029/2010JA015602>
- Basu B (2002) On the linear theory of equatorial plasma instability: comparison of different descriptions. *J Geophys Res* 107(A8):1199. <https://doi.org/10.1029/2001JA000317>
- Basu S, Basu S, Rich FJ, Groves KM, MacKenzie E, Coker C, Sahai Y, Fagundes PR, Becker-Guedes F (2007) Response of the equatorial ionosphere at dusk to penetrating electric fields during intense magnetic storms. *J Geophys Res* 112:A08308. <https://doi.org/10.1029/2006JA012192>
- Burke WJ, Gentile LC, Huang CY, Valladares CE, Su SY (2004a) Longitudinal variability of equatorial plasma bubbles observed by DMSP and ROCSAT-1. *J Geophys Res* 109:A12301. <https://doi.org/10.1029/2004JA010583>
- Burke WJ, Huang CY, Gentile LC, Bauer L (2004b) Seasonal-longitudinal variability of equatorial plasma bubbles. *Ann Geophys* 22:3089–3098
- Carter BA, Retterer JM, Yizengaw E, Groves K, Caton R, McNamara L, Bridgwood C, Francis M, Terkildsen M, Norman R, Zhang K (2014a) Geomagnetic control of equatorial plasma bubble activity modeled by the TIEGCM with K_p . *Geophys Res Lett* 41:5331–5339. <https://doi.org/10.1002/2014GL060953>
- Carter BA, Yizengaw E, Retterer JM, Francis M, Terkildsen M, Marshall R, Norman R, Zhang K (2014b) An analysis of the quiet time day-to-day variability in the

- formation of postsunset equatorial plasma bubbles in the southeast Asian region. *J Geophys Res Space Physics* 119:3206–3223. <https://doi.org/10.1002/2013JA019570>
- Dao T, Otsuka Y, Shiokawa K, Tulasi Ram S, Yamamoto M (2016) Altitude development of postmidnight F region field-aligned irregularities observed using equatorial atmosphere radar in Indonesia. *Geophys Res Lett* 43:1015–1022. <https://doi.org/10.1002/2015GL067432>
- Fujiwara H, Miyoshi Y (2009) Global structure of large-scale disturbances in the thermosphere produced by effects from the upper and lower regions: simulations by a whole atmosphere GCM. *Earth Planets Space* 61:463–470
- Fujiwara H, Miyoshi Y (2010) Morphological features and variations of temperature in the upper thermosphere simulated by a whole atmosphere GCM. *Ann Geophys* 28:427–437
- Fukao S, Ozawa Y, Yokoyama T, Yamamoto M, Tsunoda RT (2004) First observations of the spatial structure of F region 3-m-scale field-aligned irregularities with the equatorial atmosphere radar in Indonesia. *J Geophys Res* 109:A02304. <https://doi.org/10.1029/2003JA010096>
- Fukao S, Yokoyama T, Tayama T, Yamamoto M, Maruyama T, Saito S (2006) Eastward traverse of equatorial plasma plumes observed with the equatorial atmosphere radar in Indonesia. *Ann Geophys* 24:1411–1418. <https://doi.org/10.15194/angeo-24-1411-2006>
- Gentile LC, Burke WJ, Rich FJ (2006) A climatology of equatorial plasma bubbles from DMSF 1989–2004. *Radio Sci* 41:RS521. <https://doi.org/10.1029/2005RS003340>
- Haerendel G, Eccles JV, Cakir S (1992) Theory for modeling the equatorial evening ionosphere and the origin of the shear in horizontal plasma flow. *J Geophys Res* 97:1209–1223. <https://doi.org/10.1029/91JA02226>
- Huang CS (2011) Occurrence of equatorial plasma bubbles during intense magnetic storms. *Intl J Geophys* 2011:401858. <https://doi.org/10.1155/2011/401858>
- Huang CS, de La Beaujardiere O, Roddy PA, Hunton DE, Liu JY, Chen SP (2014) Occurrence probability and amplitude of equatorial ionospheric irregularities associated with plasma bubbles during low and moderate solar activities (2008–2012). *J Geophys Res Space Physics* 119:1186–1199. <https://doi.org/10.1002/2013JA019212>
- Huang CS, Hairston MR (2015) The postsunset vertical plasma drift and its effects on the generation of equatorial plasma bubbles observed by the C/NOFS satellite. *J Geophys Res Space Physics* 120:2263–2275. <https://doi.org/10.1002/2014JA020735>
- Huang CY, Burke WJ, Machuzak JS, Gentile LC, Sultan PJ (2002) Equatorial plasma bubbles observed by DMSF satellites during a full solar cycle: toward a global climatology. *J Geophys Res* 107(A12):1434. <https://doi.org/10.1029/2002JA009452>
- Huba JD, Joyce G (2007) Equatorial spread F modeling: multiple bifurcated structures, secondary instabilities, large density 'bite-outs,' and supersonic flows. *Geophys Res Lett* 34:L07105. <https://doi.org/10.1029/2006GL028519>
- Jin H, Miyoshi Y, Fujiwara H, Shinagawa H (2008) Electrodynamics of the formation of ionospheric wave number 4 longitudinal structure. *J Geophys Res* 113:A09307. <https://doi.org/10.1029/2008JA013301>
- Jin H, Miyoshi Y, Fujiwara H, Shinagawa H, Terada K, Terada N, Ishii M, Otsuka Y, Saito A (2011) Vertical connection from the tropospheric activities to the ionospheric longitudinal structure simulated by a new Earth's whole atmosphere-ionosphere coupled model. *J Geophys Res* 116:A01316. <https://doi.org/10.1029/2010JA015925>
- Jin H, Miyoshi Y, Pancheva D, Mukhtarov P, Fujiwara H, Shinagawa H (2012) Response of migrating tides to the stratospheric sudden warming in 2009 and their effects on the ionosphere studied by a whole atmosphere-ionosphere model GAIA with COSMIC and TIMED/SABER observations. *J Geophys Res* 117:A10323. <https://doi.org/10.1029/2012JA017650>
- Kil H, Paxton LJ, Oh SJ (2009) Global bubble distribution seen from ROCSAT-1 and its association with the evening prereversal enhancement. *J Geophys Res* 114:A06307. <https://doi.org/10.1029/2008JA013672>
- Miyoshi Y, Fujiwara H (2003) Day-to-day variations of migrating diurnal tide simulated by a GCM from the ground surface to the exobase. *Geophys Res Lett* 30(15):1789. <https://doi.org/10.1029/2003GL017695>
- Miyoshi Y, Fujiwara H (2006) Excitation mechanism of intraseasonal oscillation in the equatorial mesosphere and lower thermosphere. *J Geophys Res* 111: D14108. <https://doi.org/10.1029/2005JD006993>
- Miyoshi Y, Fujiwara H (2008) Gravity waves in the thermosphere simulated by a general circulation model. *J Geophys Res* 113:D01101. <https://doi.org/10.1029/2007JD008874>
- Miyoshi Y, Fujiwara H, Jin H, Shinagawa H (2014) A global view of gravity waves in the thermosphere simulated by a general circulation model. *J Geophys Res Space Physics* 119:5807–5820. <https://doi.org/10.1002/2014JA019848>
- Miyoshi Y, Fujiwara H, Jin H, Shinagawa H, Liu H (2012) Wave-4 structure of the neutral density in the thermosphere and its relation to atmospheric tides. *J Atmos Sol-Terr Phys* 90:91:45–51. <https://doi.org/10.1016/j.jastp.2011.12.002>
- Miyoshi Y, Pancheva D, Mukhtarov P, Jin H, Fujiwara H, Shinagawa H (2017) Excitation mechanism of non-migrating tides. *J Atmos Sol-Terr Phys* 156:24–36. <https://doi.org/10.1016/j.jastp.2017.02.012>
- Nishioka M, Otsuka Y, Shiokawa K, Tsugawa T, Effendy, Supnithi P, Nagatsuma T, Murata KT (2012) On post-midnight field-aligned irregularities observed with a 30.8-MHz radar at a low latitude: comparison with F-layer altitude near the geomagnetic equator. *J Geophys Res* 117:A08337. <https://doi.org/10.1029/2012JA017692>
- Nishioka M, Saito A, Tsugawa T (2008) Occurrence characteristics of plasma bubble derived from global groundbased GPS receiver networks. *J Geophys Res* 113:A05301. <https://doi.org/10.1029/2007JA012605>
- Ogawa T, Miyoshi Y, Otsuka Y, Nakamura T, Shiokawa K (2009) Equatorial GPS ionospheric scintillations over Kototabang, Indonesia and their relation to atmospheric waves from below. *Earth Planets Space* 61:397–410
- Ossakow SL, Zalesak ST, McDonald BE, Chaturvedi PK (1979) Nonlinear equatorial spread F: dependence on altitude of the F peak and bottomside background electron density gradient scale length. *J Geophys Res* 84:17–29
- Otsuka Y, Ogawa T, Effendy (2009) VHF radar observations of nighttime F-region field-aligned irregularities over Kototabang, Indonesia. *Earth Planets Space* 61:431–437
- Otsuka Y, Shiokawa K, Nishioka M, Effendy (2012) VHF radar observations of post-midnight F-region field-aligned irregularities over Indonesia during solar minimum. *Indian J Radio Space Phys* 41:199–207
- Otsuka Y, Shiokawa K, Ogawa T (2006) Equatorial ionospheric scintillations and zonal irregularity drifts observed with closely-spaced GPS receivers in Indonesia. *J Meteor Soc Jpn* 84A:343–351
- Otsuka Y, Shiokawa K, Ogawa T, Yokoyama T, Yamamoto M, Fukao S (2004) Spatial relationship of equatorial plasma bubbles and field-aligned irregularities observed with an all-sky airglow imager and the equatorial atmosphere radar. *Geophys Res Lett* 31:L20802. <https://doi.org/10.1029/2004GL020869>
- Ott E (1978) Theory of Rayleigh-Taylor bubbles in the equatorial ionosphere. *J Geophys Res* 83:2066
- Richmond AD, Ridley EC, Roble RG (1992) A thermosphere/ionosphere general circulation model with coupled electrodynamics. *Geophys Res Lett* 19:601–604. <https://doi.org/10.1029/92GL00401>
- Scannapieco AJ, Ossakow SL (1976) Nonlinear equatorial spread F. *Geophys Res Lett* 3:451–454
- Sreeja V (2016) Impact and mitigation of space weather effects on GNSS receiver performance. *Geosci Lett* 3:24. <https://doi.org/10.1186/s40562-016-0057-0>
- Steenburgh RA, Smithro CG, Groves KM (2008) Ionospheric scintillation effects on single frequency GPS. *Space Weather* 6:S04D02. <https://doi.org/10.1029/2007SW000340>
- Sultan PJ (1996) Linear theory and modeling of the Rayleigh-Taylor instability leading to the occurrence of the equatorial spread F. *J Geophys Res* 101: 26,875–26,891. <https://doi.org/10.1029/96JA00682>
- Tulasi Ram S, Rama Rao PVS, Prasad DSV, Niranjan K, Gopi Krishna S, Sridharan R, Ravindran S (2008) Local time dependent response of post sunset ESF during geomagnetic storms. *J Geophys Res* 113:A07310. <https://doi.org/10.1029/2007JA012922>
- Watanabe S, Oya H (1986) Occurrence characteristics of low latitude ionosphere irregularities observed by impedance probe on board the Hinotori satellite. *J Geomag Geoelec* 38:125–149
- Woodman RF, LaHoz C (1976) Radar observations of F region equatorial irregularities. *J Geophys Res* 81:5447–5466
- Wu Q (2015) Longitudinal and seasonal variation of the equatorial flux tube integrated Rayleigh-Taylor instability growth rate. *J Geophys Res Space Physics* 120:7952–7957. <https://doi.org/10.1002/2015JA021553>
- Wu Q (2017) Solar effect on the Rayleigh-Taylor instability growth rate as simulated by the NCAR TIEGCM. *J Atmos Sol-Terr Phys* 156:97–102
- Yokoyama T, Jin H, Shinagawa H (2015) West wall structuring of equatorial plasma bubbles simulated by three-dimensional HIRB model. *J Geophys Res Space Physics* 120. doi:<https://doi.org/10.1002/2015JA021799-T>

Yokoyama T, Shinagawa H, Jin H (2014) Nonlinear growth, bifurcation and pinching of equatorial plasma bubble simulated by three-dimensional high-resolution bubble model. *J Geophys Res Space Physics* 119:10,474–10,482. <https://doi.org/10.1002/2014JA020708>

Zalesak ST, Ossakow SL, Chaturvedi PK (1982) Nonlinear equatorial spread F: the effect of neutral winds and background conductivity. *J Geophys Res* 87:151–166

Submit your manuscript to a SpringerOpen[®] journal and benefit from:

- ▶ Convenient online submission
- ▶ Rigorous peer review
- ▶ Open access: articles freely available online
- ▶ High visibility within the field
- ▶ Retaining the copyright to your article

Submit your next manuscript at ▶ springeropen.com
